Nano Energy 90 (2021) 106522

Contents lists available at ScienceDirect

Nano Energy

journal homepage: www.elsevier.com/locate/nanoen

Hybrid printing of wearable piezoelectric sensors

Yipu Du [a,1], Ruoxing Wang [b,c,d,e,1], Minxiang Zeng [a], Shujia Xu [b,c,d,e], Mortaza Saeidi-Javash [a], Wenzhuo Wu [b,c,d,e,*], Yanliang Zhang [a,**]

[a] Department of Aerospace and Mechanical Engineering, University of Notre Dame, Notre Dame, IN 46556, USA
[b] School of Industrial Engineering, Purdue University, West Lafayette, IN 47907, USA
[c] Flex Laboratory, Purdue University, West Lafayette, IN 47907, USA
[d] Birck Nanotechnology Center, Purdue University, West Lafayette, IN 47907, USA
[e] Regenstrief Center for Healthcare Engineering, West Lafayette, IN 47907, USA

ARTICLE INFO

Keywords:
Additive manufacturing
Piezoelectricity
Tellurium nanowire
Wearable sensor

ABSTRACT

Piezoelectricity provides an ideal electromechanical mechanism with emerging applications in wearable devices due to its simplicity and self-powered nature. However, the 3D printing of piezoelectric devices still faces many challenges, including material printability, high energy poling process, and low dimensional accuracy. This study demonstrates, for the first time, a tellurium nanowire-based piezoelectric device fabricated by a hybrid printing method integrating highly complementary aerosol jet printing and extrusion printing in a single printing platform. The aerosol-jet-printed tellurium nanowire demonstrates piezoelectric properties without the need for any poling processing due to the unique properties of the tellurium nanowires. The silver nanowire electrodes printed by aerosol jet printing demonstrate excellent conductivity and stretchability without the need for sintering. An extrusion method is employed to print the silicone films, which serve as the stretchable substrate and the electrical insulation layers between the printed tellurium and silver. The printed wearable piezoelectric devices were attached to a human wrist to detect different hand gestures and to a human neck to detect heartbeat without using an external power source. The fully printed, sintering-free and poling-free, and stretchable piezoelectric device opens enormous opportunities for facile integration with a broad range of printed electronics and wearable devices.

1. Introduction

The conversion from mechanical signals to electrical signals can be achieved based on various principles, including piezoresistivity, capacitance, piezoelectricity, and triboelectricity [1–3]. Among them, piezoelectricity is one of the promising mechanisms used in wearable electronics, mainly due to its capability of realizing self-powered, highly sensitive, and fast response devices [4–9]. In recent years, 3D printing technology, which is known for its flexibility and rapid prototyping capability, has been utilized to fabricate wearable piezoelectric nanogenerators (PENG) [10–13].

Although various 3D printing methods are highly accessible nowadays, the limited choice of printable material has historically been a concern for many printing processes. The most widely used piezoelectric materials for 3D printing are characterized as ceramics, polymers, and composites [11]. Direct printing of ceramics is challenging due to the high stiffness and high melting point [14]. One printing strategy is to formulate solution-based ceramic nanoparticles [14,15]. However, this method is limited by the requirement for high sintering temperature and high electric fields for poling. With low processing temperature and high printability, piezoelectric polymers are more frequently used in 3D printing [11,16]. The most common piezoelectric polymers include semi-crystalline polyvinylidene fluoride (PVDF) and its copolymer polyvinylidene fluoride-trifluoroethylene (PVDF-TrFE) [17–19], which can be printed using fused filament fabrication. The poling process can be performed during printing[20,21] by applying a high electric field between the nozzle tip and printing bed to transform the PVDF molecular chain to β-phase, or after printing [22–24]. In some cases, electrohydrodynamic printing is applied to print PVDF nanofibers [25,26]. Although the piezoelectric polymer has improved printability compared

* Corresponding author at: School of Industrial Engineering, Purdue University, West Lafayette, IN 47907, USA.
** Corresponding author.
E-mail addresses: wenzhuowu@purdue.edu (W. Wu), yzhang45@nd.edu (Y. Zhang).
[1] The authors contribute equally.

https://doi.org/10.1016/j.nanoen.2021.106522
Received 12 July 2021; Received in revised form 2 September 2021; Accepted 11 September 2021
Available online 16 September 2021

to ceramics-based ink, the drawbacks include low dimensional accuracy and low piezoelectric response. Even with the poling process, there are still concerns about transforming back to the thermodynamically stable nonpolar phase upon solidification. To address these issues and improve the piezoelectric response, piezoelectric ceramic fillers were incorporated in the polymer matrix [27–34]. For example, piezoelectric ceramic nanoparticles (e.g., BaTiO3) were mixed with photocurable polymer so that the stereolithography-based printing technology can be used to improve printability and dimensional accuracy [10,35–38]. To maximize the piezoelectric response, the stress transfer between the polymer and the filler is maximized by functionalizing the ceramic nanoparticles [12,13].

Although the printed piezoelectric devices have demonstrated decent performances, they are all based on piezoelectric compounds, where the piezoelectric charges are induced by ionic polarization [39]. This leads to the need to align the printed structures. The often-required high energy poling process significantly complicates the printing process and can be detrimental to the surrounding materials during the sensor integration process [40]. In addition, the fabrication of piezoelectric devices requires multiple materials, which often require multiple processing steps and equipment.

This work demonstrates a highly versatile and unique hybrid printing process to fabricate stretchable piezoelectric devices using tellurium nanowires (Te NW) and silver nanowires (Ag NW). The unique radial distribution of piezoelectric polarization in the Te NW simplifies the fabrication process by eliminating the need for high-energy post-processing (Fig. 1e) [41,42], while the Ag NW films demonstrate adequate conductivity and stretchability without the need for sintering. A custom-built hybrid printing system integrating aerosol jet printing and extrusion printing was used to directly print all the required materials into a complete piezoelectric device. The aerosol-jet-printed Te NW and Ag NW thin films serve as the active piezoelectric material and stretchable electrodes, respectively. The extrusion printed silicone films provide electrical insulation and stretchable substrates. Characterizations of the printed device are performed to prove the feasibility of the proposed method. Moreover, a wearable piezoelectric sensor is demonstrated by detecting the gesture and the pulse. Our hybrid printing method provides exciting opportunities to harmoniously integrate and transform functional materials and structural materials into a highly integrated wearable electronic system.

2. Ink formulation and drying kinetics

To ensure the smooth printing of nanomaterials, ink formulation is often of great importance. The Te NW and Ag NW were synthesized using a bottom-up wet-chemistry method [41,43,44]. The SEM images confirm the shape and morphology of Te NW and Ag NW as shown in Fig. 1c-d. Then, Te NW and Ag NW are redispersed in solvents to formulate printable nanowire inks. It is interesting to find that the Ag NW ink shows strong liquid-crystalline birefringence (Fig. 2**c**). Such lyotropic self-alignment feature is an indicator of high aspect ratio (length-to-diameter) and relatively low polydispersity [45], which is reminiscent of molecular liquid crystal rod systems, such as 4-cyano-4′-pentylbiphenyl (5CB) [46]. To understand the collective behavior of silver nanowire inks, we first investigated the effect of ink solvent, including water, isopropyl alcohol (IPA), and dimethylformamide

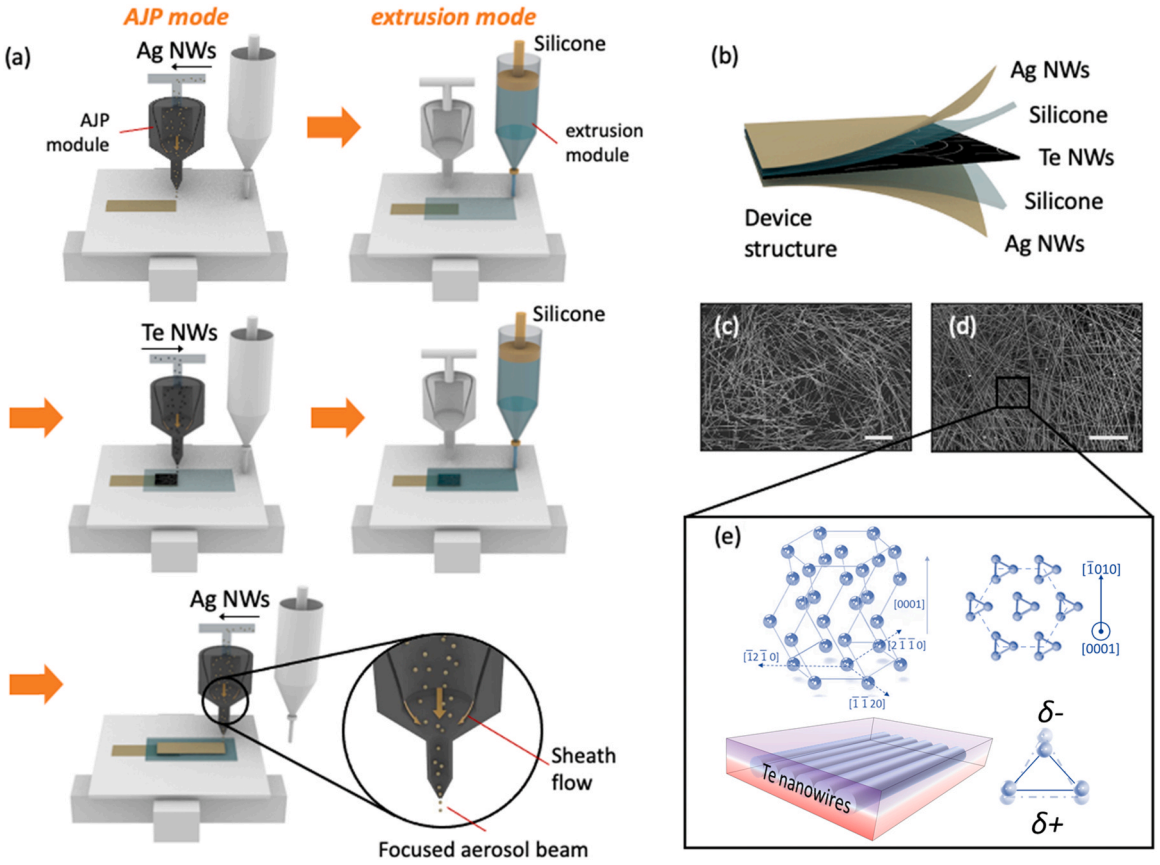

Fig. 1. (a) The hybrid printing process of the piezoelectric device using the aerosol jet printer module (left) and the extrusion printing module (right). The inactive component in each step is in white color. The subgraph shows the deposition mechanism of the aerosol jet printing head, where the arrows in gold color represent the direction of the sheath flow and the spheres in yellow color represent the ink droplets. (b) The structure of the printed piezoelectric device. (c) The SEM image of silver nanowires before printing. The scale bar is 1 μm. (d) The SEM image of tellurium nanowires before printing. The scale bar is 1 μm. (e) The atomic structure of Te nanowires and the piezoelectric potential distribution (indicated by the color gradient) in the radial direction of Te nanowires encapsulated in silicone layers.

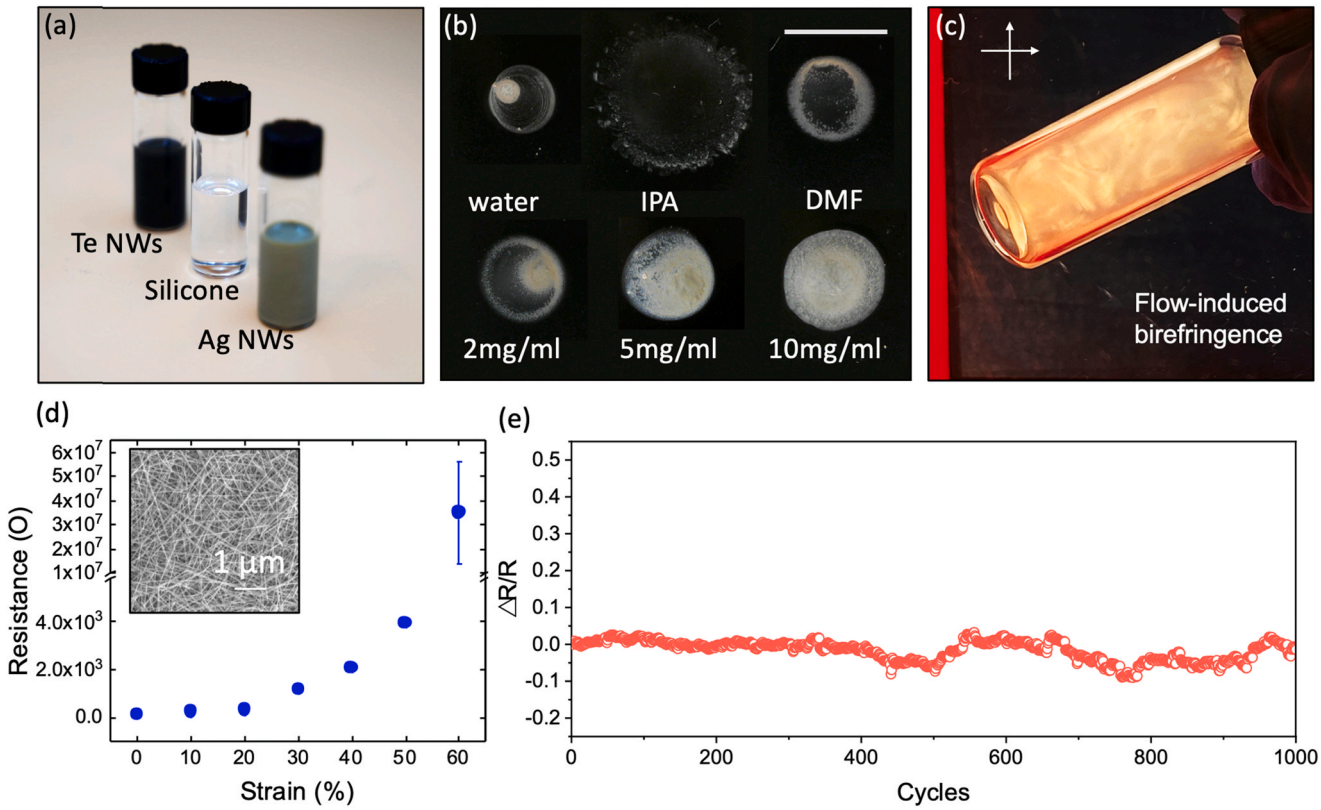

Fig. 2. (a) The inks used in the hybrid printing of the piezoelectric device. (b) The coffee ring effect of the silver nanowire ink dropped on glass slides. The scale bar is 1 cm. (c) The flow-induced birefringence property of the silver nanowire ink. (d) The resistance change of the printed silver nanowire film (1 by 20 mm) under different tensile strains. The subgraph is the SEM image of the printed silver nanowire film. (e) The stability curve of the printed silver nanowire film (1 by 20 mm) under 20% strain for 1000 cycles.

(DMF), on film deposition (Fig. 2b). For Ag nanowire ink, the water-based ink shows large aggregates in the dried film and thus is not suitable for printing. The IPA-based ink shows a relatively uniform film after drying. However, it cannot generate a stable aerosol stream using our printer, which is likely due to the high volatility of IPA that causes the early breakup of aerosol droplets. Although the DMF-based ink shows a noticeable coffee-ring effect where the middle region of the dried film is depleted of NW particles, we found that a higher nanowire concentration (>5 mg/mL) can mitigate such undesired phenomena [47]. In fact, ink concentration plays an essential role in the nanoparticle percolation, as a low solid content means slower drying kinetics and pronounced drying effects (such as the coffee-ring effect) [48]. It is worth mentioning that an extremely high ink concentration may not be suitable for printing due to increased ink viscosity and possible particle agglomeration. As shown in Fig. 2b, an increase in Ag NW concentration in DMF leads to significant improvements in particle percolation and film uniformity.[43].

3. Hybrid printing process of piezoelectric devices

A hybrid additive manufacturing process integrating extrusion printing and multi-material aerosol jet printing (MMAJP) was developed for printing both functional and structural materials in order to form a complete piezoelectric device. The fabrication process is shown in Fig. 1a. The extrusion printing module has a pneumatic system providing pressure controlled by solenoid valves to extrude viscous silicone ink out of a syringe to form a stretchable electrical insulation layer. A UV curable silicone ink (SEMICOSIL 949 UV A/B) with relatively low viscosity was used to fabricate the thin insulation layer. The MMAJP was designed to print multiple inks at the same time without the need to change inks. The tellurium and silver nanowire inks were printed by MMAJP to form thin films of the piezoelectric layer and stretchable electrodes, respectively. During the printing process, the ink was atomized into aerosols by ultrasonic force and carried into the printing head by a nitrogen gas flow. A sheath flow was used to aerodynamically focus the ink flow into a fine beam to achieve high spatial resolution and enable 3D conformal printing on non-planar substrates [49,50]. The all-printed piezoelectric device has a layered structure (Fig. 1b). The aerosol jet printed Te NW piezoelectric layer is sandwiched between two extruded silicone layers for electrical insulation. The aerosol-jet-printed Ag NW electrodes are on the top and the bottom to conduct the generated electric signal.

4. Properties of the printed silver nanowire electrodes

Silver nanowires are chosen for printing electrodes due to the high conductivity and stretchability as a result of the silver nanowire percolation network [51,52]. The conductivity of the printed Ag NW electrodes can reach 3.4×10^5 S/m for a single layer and 7.4×10^5 S/m for three layers without the need for sintering, which is sufficient to be used for a piezoelectric device. The resistance versus tensile strain of a printed Ag NW film on silicone is shown in Fig. 2d. The electrode remains conductive under up to 50% strain and can recover to the initial state. The stability curve of the printed Ag NW film under 20% strain is shown in Fig. 2e. The printed silver nanowires electrode shows good stability with relative resistance change lower than 10% after 1000 stretching-releasing cycles. The change of resistance remains negligible compared to the total resistance of the piezoelectric device. During the atomizing process, long silver nanowires with the original length of 20–40 μm are converted into shorter pieces of 1–5 μm (Fig. 2d) to enable the generation of aerosols carrying the nanowires.

5. Piezoelectric device performances

The piezoelectric outputs of the all-printed and stretchable devices were investigated to illustrate the sensing and energy harvesting performances. Based on the crystal structure of Te NW, the projection of the helical chains with equilateral triangles of Te atoms onto the (0 0 0 1) plane is shown in Fig. 1e [42]. The non-centrosymmetric structure of Te leads to its piezoelectric property, where an individual helical chain is constructed of strong covalent bonds while adjacent chains are stacked by interchain interactions that are weaker than the covalent bond forming a hexagonal lattice [53]. The piezoelectric constant e_{11} could be divided orthogonally into e_x and e_y, perpendicular and parallel to the substrate, respectively [39]. When an external strain is applied along the radial direction (e_x) of a Te NW, the shape of the equilateral triangle distorts, resulting in a relative displacement of the electron distribution against the Te atoms cores, leading to piezoelectric polarization as shown in Fig. 1e [41,42]. Thus, the piezoelectric potential would be generated from printed Te NWs on substrates under strain along the [$\bar{1}$010] direction. When the substrate was stretched mechanically, a corresponding contraction must occur along the perpendicular axis with Poisson's ratio, giving rise to the compressive strain along the nanowires' radial directions. The generated piezo-charges induced opposite charges in the printed Ag NW electrodes, resulting in a potential difference between the two electrodes and driving electrons to flow in the external circuit. When the applied strain was released, the piezoelectric potential vanished immediately and the electrons flowed back to reach the electrostatic equilibrium [54]. Electrical pulses were generated by periodically repeating the stretching-releasing process. The typical results of open-circuit voltage and short-circuit current generated from an all-printed Te NW piezoelectric device are shown in Fig. 3a and b, respectively. Statistical results for the piezoelectric outputs from an all-printed Te NW piezoelectric device with different strain loading are shown in Fig. 3c. It can be seen that both the generated voltages and currents are strain-dependent, which increased with larger strain loading, agreeing well with the previously reported results [41,55]. When the applied strain was larger than 50%, the resistance of printed Ag NW electrodes increased dramatically (Fig. 2d), preventing the efficient collection of piezoelectric signals. The stretchability of 50% has also surpassed that of biological skin (~30%), indicating the capability of all-printed Te NW piezoelectric devices for wearable applications [56]. Besides, the output power with different external load resistances was measured at 20% strain (Fig. 3d). The optimized output power of 32.1 nW/m^2 was achieved with 1 GΩ external load. The stability test of the all-printed Te NW piezoelectric device is shown in Fig. 3e. The open-circuit voltages have a typical square wave shape without noticeable degradation over 1000 s through continuous stretching-releasing processes (0.8 Hz), indicating the excellent mechanical durability of the device.

To demonstrate the wearability and sensitivity of the printed piezoelectric device, we attached the device to a human wrist to detect different hand gestures and to a human neck to detect heartbeat without using an external power source. In Fig. 4a-d, the piezoelectric signals are shown based on four different hand gestures, which were measured by the same all-printed device. The wearable device attached to the wrist was deformed due to the movement of the underlying tendons and muscles and generated corresponding signals [57]. For the same gesture, the waveforms have good repeatability. Moreover, the waveforms are significantly distinguishable among different gestures, indicating a high resolution of tiny movements from the underlying tendons and muscles. Therefore, the all-printed wearable piezoelectric devices have great potential in detecting subtle muscle movement for diagnostics, rehabilitation, and human-machine-interface applications [58–63]. In addition, the wearable device was attached to the human neck to explore its feasibility to detect imperceptible movement of blood vessel expansion due to the blood ejection from the heart. In Fig. 4e, the real-time piezoelectric signals from the wearable device show the reliable detection and measurement of human heartbeats. The peaks labeled by red bars are corresponding to the heartbeats. The heart rate

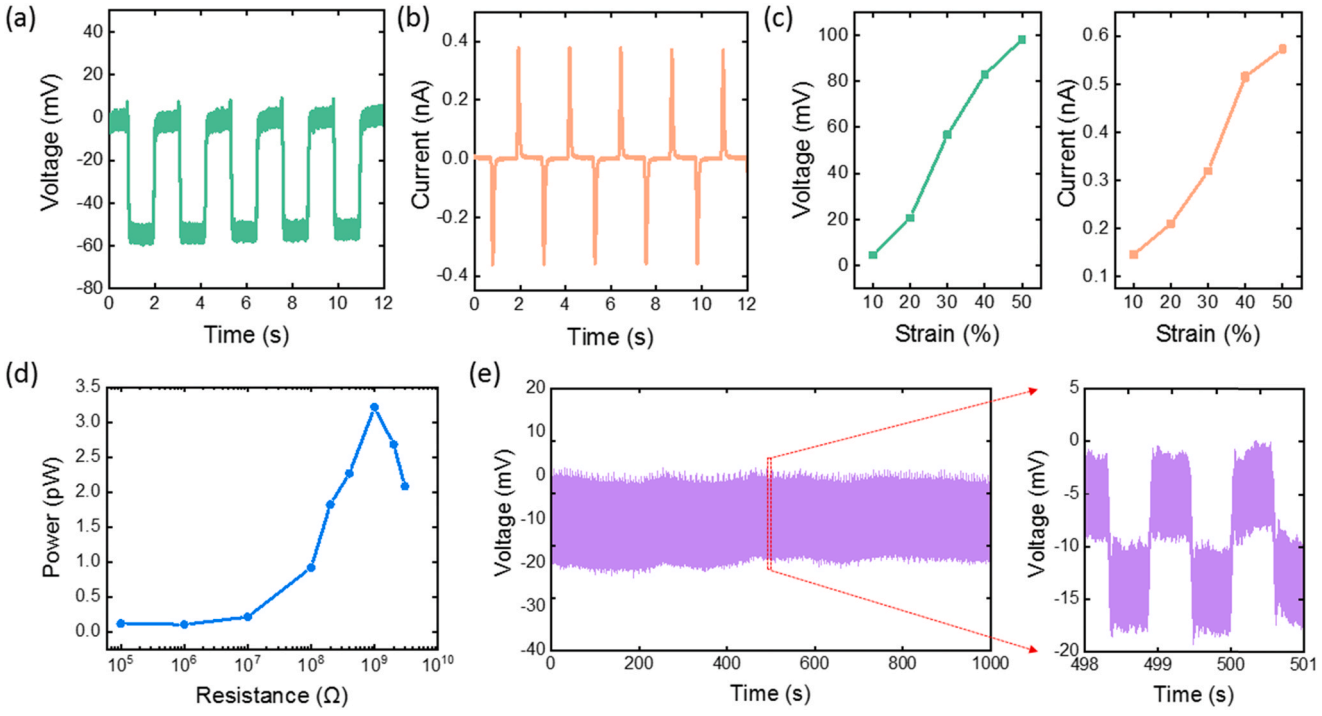

Fig. 3. The characterization of the all-printed piezoelectric device. (a) The typical result of open-circuit voltage generated from the all-printed piezoelectric device. (b) The typical result of short-circuit current generated from the all-printed piezoelectric device. (c) The statistical result of the open-circuit voltage (left) and the short-circuit current (right) from the all-printed piezoelectric device under different strain. (d) The output power with different external load resistance under 20% strain. (e) The stability curve of the all-printed piezoelectric device. The magnified view is displayed on the right.

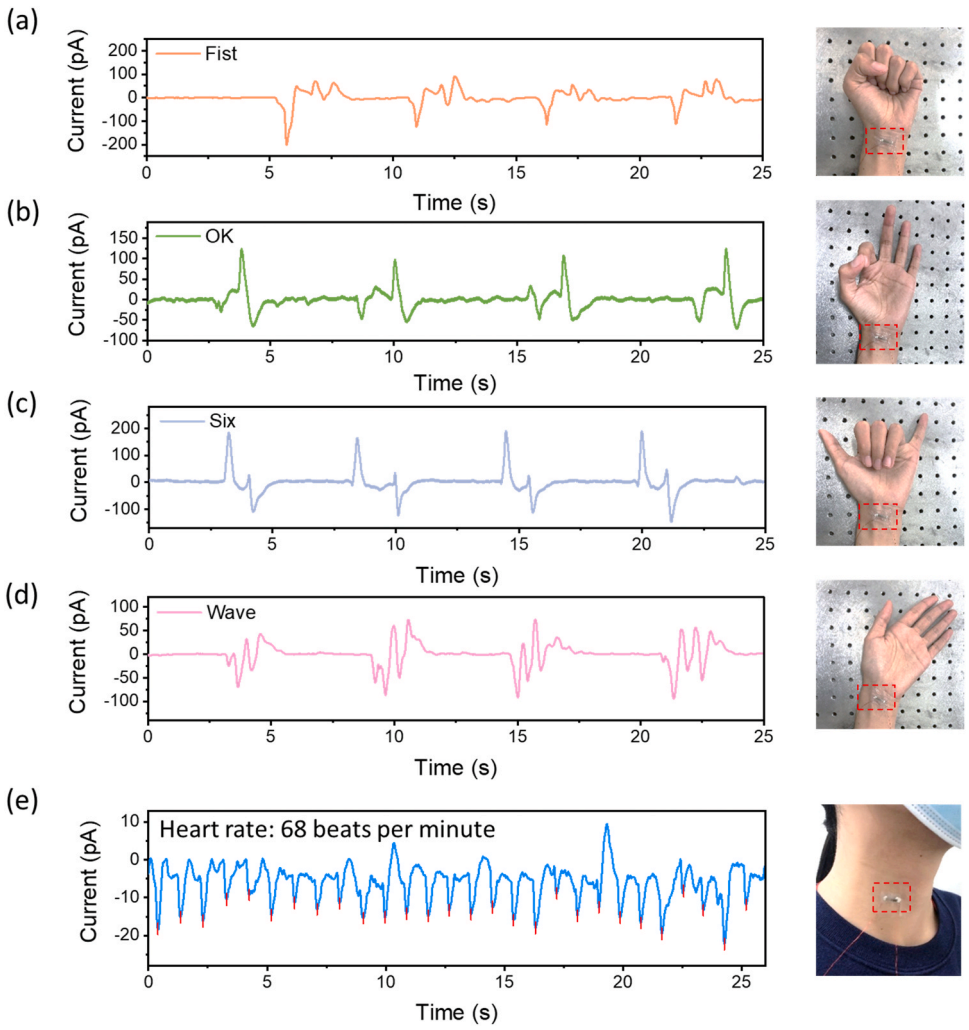

Fig. 4. The demonstration of the wearability and sensitivity of the all-printed piezoelectric device. (a)-(d) The piezoelectric signal generated from the all-printed piezoelectric device attached on the wrist when different gestures are made. (e) The piezoelectric signal generated from the all-printed device attached on the neck indicating the human heartbeat.

can be measured by counting the peak numbers within one minute. The highly customizable platform enabled by hybrid 3D printing along with the demonstrated capability of sensing physiological biomechanical signals can be applied to broader wearable and biomedical applications [64–66].

6. Conclusion

In summary, a fully printed stretchable and wearable piezoelectric sensor is demonstrated using a hybrid 3D printing strategy. Owing to the nanowire network formed during printing, we found that the printed nanowire-based electrodes and piezoelectric devices reveal excellent intrinsic stretchability without sophisticated design requirements (e.g., serpentine patterns). In addition, no high-temperature sintering or high voltage poling processes are necessitated in our proposed approach, which facilities direct device printing on temperature/voltage sensitive components, providing opportunities for facile integration of piezoelectric devices into the future highly integrated printed electronics and wearable devices. The printed wearable piezoelectric devices could efficiently convert the imperceptible mechanical movements from the human body into distinguishable electrical signals through straining the piezoelectric Te nanowires. This study of hybrid 3D printed wearable piezoelectric sensors can be potentially expanded to various materials and structures due to the highly customizable platform, providing a new strategy for the fabrication of wearable and biomedical sensors.

7. Experimental section

7.1. Synthesis of Te nanowire and Ag nanowire

Tellurium (Te) nanowires were synthesized by the hydrothermal method as described in the previous report [41,43]. Typically, 0.4 mmol Na_2TeO_3 and 1 g PVP (M. W. = 58,000) were added into deionized (DI) water with magnetic stirring until fully dissolved. The solution was transferred into a Teflon vessel which was then filled with aqueous ammonia solution and hydrazine hydrate. The autoclave was sealed and maintained at 180 °C for 3 h and cooled down to room temperature rapidly by cold tap water. The obtained black products were washed with DI water and acetone three times.

Silver (Ag) nanowires were synthesized by a seed-assisted solution-based method following the procedures reported in the previous work [44]. Ethylene glycol (EG) was applied in all solutions as solvent. The Ag seed solution was prepared by mixing 5 mL EG, 1 mL 100 mM polyvinylpyrrolidone (PVP, M.W. = 40,000), 136 μL 25 mg/mL silver nitrate ($AgNO_3$) and 50 μL 220 mM sodium bromide (NaBr) in a glass vial. The seed solution was maintained at 130 °C for 15 min and cooled down to room temperature naturally. The growth solution of Ag nanowires was prepared by mixing 5 mL EG, 5 mL 25 mg/mL $AgNO_3$, 5 mL 20 mg/mL

PVP (M.W. = 360,000), 0.5 mL 100 mM sodium chloride (NaCl) and 0.5 mL Ag seed solution in a Teflon vessel. The autoclave was sealed and maintained at 150 °C for 6 h and cooled down to room temperature rapidly by cold tap water. The obtained products were washed with acetone for several times.

7.2. Ink formulation

Tellurium nanowires are dispersed in water to formulate Te NW inks. Silver nanowires are subject to a solvent exchange process that allows the Ag nanowires to be dispersed in DMF. All nanowires are subjected to mild bath sonication prior to the printing process. The silicone ink (SEMICOSIL 949 UV A/B) used to fabricate the insulation layers was purchased from WACKER. The component A and component B were thoroughly mixed with a 2–1 ratio before printing. The viscosity of component A is 150.0 mPa·s and is 1000.0 mPa·s for component B. The silicone ink (SYLGARD 184, Dow) was used to fabricate the substrates.

7.3. Device printing

7.3.1. Printing of silver nanowire ink

During aerosol jet printing, a 20-gauge nozzle was used in the AJP module to print silver nanowire. The printing speed was 2 mm/s, and during the printing process, the platform temperature was kept at 83 ℃ while the sonicating base was kept at 27 ℃. The sheath flow rate and the ink flow rate were set to be 70 and 20 SCCM, respectively. The atomizer voltage was set at 35 volts. 3 layers of silver nanowire were printed to form the bottom electrodes and 5 layers were printed to form the top electrodes to avoid the step effect. After the bottom electrodes were printed and dried on an 83 ℃ hotplate for 20 min, the insulation silicone ink was directly printed on the top.

7.3.2. Printing of silicone ink

The silicone ink used in the insulation layer was printed by a customized extrusion printing module with a 26 gauge nozzle. During printing, the extrusion pressure, the printing speed and the distance between the nozzle tip were maintained at 1.5 bar, 5 mm/s and 0.3 mm, respectively. The printed layer was then cured under a 365 nm UV LED (SkyBeam UV4053–365F, Uvitron International) for 15 min. Further, the cured layer was plasma treated for 2 min to obtain a hydrophilic surface which enables the smooth deposition of aerosol ink.

7.3.3. Printing of piezoelectric tellurium nanowire ink

The Te NW ink was also printed by the aerosol jet printing module with a 20 gauge nozzle. The ink was diluted to 4 mg/mL before printing. The hotplate was kept at 80 ℃ while the atomizer voltage was set to 31 volts. The sheath flow and ink flow were set as 60 SCCM and 18 SCCM. 6 layers were printed to ensure sufficient coverage over the substrate.

7.4. Device characterization

A linear motor (LinMot PS01–23 × 80) was applied to stretch the samples with controlled strains (maximum speed, 1 m s^{-1}; acceleration, 1 m s^{-2}; deceleration, 1 m s^{-2}). The resistances of printed Ag NW electrodes were characterized by using a function generator (Stanford Research System, DS345). Piezoelectric outputs from the all-printed Te NW devices were measured by an electrometer (Keithley 6514) and a low current preamplifier (Stanford Research System, SR570). Real-time data acquisition was performed on a LabVIEW-based software platform. The gesture and heartbeat measurements were performed following the protocol approved by the Purdue Institutional Review Board (IRB No. 1809021076).

CRediT authorship contribution statement

Yanliang Zhang and Wenzhuo Wu conceived the idea and supervised the project. Wenzhuo Wu, Yanliang Zhang, Yipu Du, and Ruoxing Wang designed the experiments. Ruoxing Wang, Shujia Xu synthesized Te nanowire samples. Minxiang Zeng formulated the printable inks. Yipu Du built the printer, developed the fabrication process and fabricated the devices. Ruoxing Wang and Minxiang Zeng helped in the SEM, XRD, and Raman measurements. Ruoxing Wang and Yipu Du analyzed the data under the guidance of Wenzhuo Wu and Yanliang Zhang. Yanliang Zhang, Wenzhuo Wu, Yipu Du, and Ruoxing Wang wrote the manuscript. All authors have discussed the results and commented on the paper.

Declaration of Competing Interest

The authors declare that they have no known competing financial interests or personal relationships that could have appeared to influence the work reported in this paper.

Acknowledgments

Yanliang Zhang would like to acknowledge funding support from the National Science Foundation under award CMMI-1747685, and the U.S. Department of Energy under award DE-NE0008712. Wenzhuo Wu acknowledges the School of Industrial Engineering at Purdue University for the Ravi and Eleanor Talwar Rising Star Professorship support. The synthesis of the tellurium nanowires was supported by National Science Foundation under grant no. CMMI-1762698.

Appendix A. Supporting information

Supplementary data associated with this article can be found in the online version at doi:10.1016/j.nanoen.2021.106522.

References

[1] A. Chortos, J. Liu, Z. Bao, Pursuing prosthetic electronic skin, Nat. Mater. 15 (2016) 937–950, https://doi.org/10.1038/nmat4671.
[2] J.C. Yang, J. Mun, S.Y. Kwon, S. Park, Z. Bao, S. Park, Electronic skin: recent progress and future prospects for skin-attachable devices for health monitoring, robotics, and prosthetics, Adv. Mater. 31 (2019) 1904765, https://doi.org/10.1002/adma.201904765.
[3] W. Wu, L. Wang, Y. Li, F. Zhang, L. Lin, S. Niu, D. Chenet, X. Zhang, Y. Hao, T. F. Heinz, J. Hone, Z.L. Wang, Piezoelectricity of single-atomic-layer MoS2 for energy conversion and piezotronics, Nature 514 (2014) 470–474, https://doi.org/10.1038/nature13792.
[4] Z. Chen, Z. Wang, X. Li, Y. Lin, N. Luo, M. Long, N. Zhao, J.-B. Xu, Flexible piezoelectric-induced pressure sensors for static measurements based on nanowires/graphene heterostructures, ACS Nano 11 (2017) 4507–4513, https://doi.org/10.1021/acsnano.6b08027.
[5] Y. Zhou, J. He, H. Wang, K. Qi, N. Nan, X. You, W. Shao, L. Wang, B. Ding, S. Cui, Highly sensitive, self-powered and wearable electronic skin based on pressure-sensitive nanofiber woven fabric sensor, Sci. Rep. 7 (2017) 12949, https://doi.org/10.1038/s41598-017-13281-8.
[6] S. Lim, D. Son, J. Kim, Y.B. Lee, J. Song, S. Choi, D.J. Lee, J.H. Kim, M. Lee, T. Hyeon, D. Kim, Transparent and stretchable interactive human machine interface based on patterned graphene heterostructures, Adv. Funct. Mater. 25 (2015) 375–383, https://doi.org/10.1002/adfm.201402987.
[7] M. Ha, S. Lim, J. Park, D. Um, Y. Lee, H. Ko, Bioinspired interlocked and hierarchical design of ZnO nanowire arrays for static and dynamic pressure-sensitive electronic skins, Adv. Funct. Mater. 25 (2015) 2841–2849, https://doi.org/10.1002/adfm.201500453.
[8] H.G. Yeo, T. Xue, S. Roundy, X. Ma, C. Rahn, S. Trolier-McKinstry, Strongly (001) oriented bimorph PZT film on metal foils grown by rf-sputtering for wrist-worn piezoelectric energy harvesters, Adv. Funct. Mater. 28 (2018) 1801327, https://doi.org/10.1002/adfm.201801327.
[9] M. Mariello, L. Fachechi, F. Guido, M.D. Vittorio, Conformal, ultra-thin skin-contact-actuated hybrid piezo/triboelectric wearable sensor based on AlN and parylene-encapsulated elastomeric blend, Adv. Funct. Mater. 31 (2021) 2101047, https://doi.org/10.1002/adfm.202101047.
[10] K. Kim, W. Zhu, X. Qu, C. Aaronson, W.R. McCall, S. Chen, D.J. Sirbuly, 3D optical printing of piezoelectric nanoparticle-polymer composite materials, ACS Nano 8 (2014) 9799–9806, https://doi.org/10.1021/nn503268f.
[11] E.R. Cholleti, A Review on 3D printing of piezoelectric materials, IOP Conf. Ser.: Mater. Sci. Eng. 455 (2018), 012046, https://doi.org/10.1088/1757-899x/455/1/012046.
[12] D. Yao, H. Cui, R. Hensleigh, P. Smith, S. Alford, D. Bernero, S. Bush, K. Mann, H. F. Wu, M. Chin-Nieh, G. Youmans, X. (Rayne) Zheng, Achieving the upper bound of

piezoelectric response in tunable, wearable 3D printed nanocomposites, Adv. Funct. Mater. 29 (2019) 1903866, https://doi.org/10.1002/adfm.201903866.
[13] H. Cui, R. Hensleigh, D. Yao, D. Maurya, P. Kumar, M.G. Kang, S. Priya, X. (Rayne) Zheng, Three-dimensional printing of piezoelectric materials with designed anisotropy and directional response, Nat. Mater. 18 (2019) 234–241, https://doi.org/10.1038/s41563-018-0268-1.
[14] B. García-Farrera, L.F. Velásquez-García, Ultrathin ceramic piezoelectric films via room-temperature electrospray deposition of ZnO nanoparticles for printed GHz devices, ACS Appl. Mater. Inter 11 (2019) 29167–29176, https://doi.org/10.1021/acsami.9b09563.
[15] X. Wei, Y. Liu, D. Zhao, S.S. Ge, 3D printing of piezoelectric barium titanate with high density from milled powders, J. Eur. Ceram. Soc. 40 (2020) 5423–5430, https://doi.org/10.1016/j.jeurceramsoc.2020.06.021.
[16] C. Chen, X. Wang, Y. Wang, D. Yang, F. Yao, W. Zhang, B. Wang, G.A. Sewvandi, D. Yang, D. Hu, Additive manufacturing of piezoelectric materials, Adv. Funct. Mater. 30 (2020) 2005141, https://doi.org/10.1002/adfm.202005141.
[17] A. Closson, H. Richards, Z. Xu, C. Jin, L. Dong, J.X.J. Zhang, Method for Inkjet-printing PEDOT:PSS polymer electrode arrays on piezoelectric PVDF-TrFE fibers, IEEE Sens. J. (2021) 1, https://doi.org/10.1109/jsen.2021.3071321.
[18] J. Kim, S. Byun, S. Lee, J. Ryu, S. Cho, C. Oh, H. Kim, K. No, S. Ryu, Y.M. Lee, S. Hong, Cost-effective and strongly integrated fabric-based wearable piezoelectric energy harvester, Nano Energy 75 (2020), 104992, https://doi.org/10.1016/j.nanoen.2020.104992.
[19] J. Ryu, J. Kim, J. Oh, S. Lim, J.Y. Sim, J.S. Jeon, K. No, S. Park, S. Hong, Intrinsically stretchable multi-functional fiber with energy harvesting and strain sensing capability, Nano Energy 55 (2019) 348–353, https://doi.org/10.1016/j.nanoen.2018.10.071.
[20] C. Lee, J.A. Tarbutton, Electric poling-assisted additive manufacturing process for PVDF polymer-based piezoelectric device applications, Smart Mater. Struct. 23 (2014), 095044, https://doi.org/10.1088/0964-1726/23/9/095044.
[21] C. Lee, J.A. Tarbutton, Electric poling-assisted additive manufacturing process for lead-free piezoelectric device fabrication, Procedia Manuf. 1 (2015) 320–326, https://doi.org/10.1016/j.promfg.2015.09.035.
[22] H. Kim, F. Torres, Y. Wu, D. Villagran, Y. Lin, T.-L. Tseng, Integrated 3D printing and corona poling process of PVDF piezoelectric films for pressure sensor application, Smart Mater. Struct. 26 (2017), 085027, https://doi.org/10.1088/1361-665x/aa738e.
[23] M. Marandi, J. Tarbutton, Additive manufacturing of single- and double-layer piezoelectric PVDF-TrFE copolymer sensors, Procedia Manuf. 34 (2019) 666–671, https://doi.org/10.1016/j.promfg.2019.06.194.
[24] X. Yuan, X. Gao, X. Shen, J. Yang, Z. Li, S. Dong, A 3D-printed, alternatively tilt-polarized PVDF-TrFE polymer with enhanced piezoelectric effect for self-powered sensor application, Nano Energy 85 (2021), 105985, https://doi.org/10.1016/j.nanoen.2021.105985.
[25] Y. Huang, Y. Ding, J. Bian, Y. Su, J. Zhou, Y. Duan, Z. Yin, Hyper-stretchable self-powered sensors based on electrohydrodynamically printed, self-similar piezoelectric nano/microfibers, Nano Energy 40 (2017) 432–439, https://doi.org/10.1016/j.nanoen.2017.07.048.
[26] Y.K. Fuh, B.S. Wang, C.-Y. Tsai, Self-powered pressure sensor with fully encapsulated 3D printed wavy substrate and highly-aligned piezoelectric fibers array, Sci. Rep. 7 (2017) 6759, https://doi.org/10.1038/s41598-017-07360-z.
[27] M. Nadgorny, A. Ameli, Functional polymers and nanocomposites for 3D printing of smart structures and devices, ACS Appl. Mater. Inter. 10 (2018) 17489–17507, https://doi.org/10.1021/acsami.8b01786.
[28] M. Gao, L. Li, W. Li, H. Zhou, Y. Song, Direct writing of patterned, lead-free nanowire aligned flexible piezoelectric device, Adv. Sci. (Weinh., Baden. -Wurtt., Ger.) 3 (2016) 1600120, https://doi.org/10.1002/advs.201600120.
[29] F. Qi, N. Chen, Q. Wang, Dielectric and piezoelectric properties in selective laser sintered polyamide11/BaTiO3/CNT ternary nanocomposites, Mater. Des. 143 (2018) 72–80, https://doi.org/10.1016/j.matdes.2018.01.050.
[30] D. Grinberg, S. Siddique, M. Le, R. Liang, J. Capsal, P. Cottinet, 4D Printing based piezoelectric composite for medical applications, J. Polym. Sci. Part B Polym. Phys. 57 (2019) 109–115, https://doi.org/10.1002/polb.24763.
[31] Z. Wang, X. Yuan, J. Yang, Y. Huan, X. Gao, Z. Li, H. Wang, S. Dong, Accuracy of virtual surgical planning-assisted management for maxillary hypoplasia in adult patients with cleft lip and palate, J. Plast., Reconstr. Aesthetic Surg.: JPRAS 73 (2020) 134–140, https://doi.org/10.1016/j.nanoen.2020.104737.
[32] C. Jin, N. Hao, Z. Xu, I. Trase, Y. Nie, L. Dong, A. Closson, Z. Chen, J.X.J. Zhang, Flexible piezoelectric nanogenerators using metal-doped ZnO-PVDF films, Sens. Actuators A, Phys. 305 (2020), 111912, https://doi.org/10.1016/j.sna.2020.111912.
[33] C. Jin, L. Dong, Z. Xu, A. Closson, A. Cabe, A. Gruslova, S. Jenney, D. Escobedo, J. Elliott, M. Zhang, N. Hao, Z. Chen, M.D. Feldman, J.X.J. Zhang, Skin-like elastomer embedded zinc oxide nanoarrays for biomechanical energy harvesting, Adv. Mater. Interfaces 8 (2021) 2100094, https://doi.org/10.1002/admi.202100094.
[34] Z. Xu, C. Jin, A. Cabe, D. Escobedo, N. Hao, I. Trase, A.B. Closson, L. Dong, Y. Nie, J. Elliott, M.D. Feldman, Z. Chen, J.X.J. Zhang, Flexible energy harvester on a pacemaker lead using multibeam piezoelectric composite thin films, ACS Appl. Mater. Interfaces 12 (2020) 34170–34179, https://doi.org/10.1021/acsami.0c07969.
[35] Z. Chen, X. Song, L. Lei, X. Chen, C. Fei, C.T. Chiu, X. Qian, T. Ma, Y. Yang, K. Shung, Y. Chen, Q. Zhou, 3D printing of piezoelectric element for energy focusing and ultrasonic sensing, Nano Energy 27 (2016) 78–86, https://doi.org/10.1016/j.nanoen.2016.06.048.
[36] J. Cheng, Y. Chen, J.-W. Wu, X.-R. Ji, S.-H. Wu, 3D printing of BaTiO3 piezoelectric ceramics for a focused ultrasonic array, Sensors 19 (2019) 4078, https://doi.org/10.3390/s19194078.
[37] Z. Chen, X. Qian, X. Song, Q. Jiang, R. Huang, Y. Yang, R. Li, K. Shung, Y. Chen, Q. Zhou, Three-dimensional printed piezoelectric array for improving acoustic field and spatial resolution in medical ultrasonic imaging, Micromachines 10 (2019) 170, https://doi.org/10.3390/mi10030170.
[38] X. Zhou, K. Parida, O. Halevi, S. Magdassi, P.S. Lee, All 3D printed stretchable piezoelectric nanogenerator for self-powered sensor application, Sensors 20 (2020) 6748, https://doi.org/10.3390/s20236748.
[39] S. Gao, Y. Wang, R. Wang, W. Wu, Piezotronic effect in 1D van der Waals solid of elemental tellurium nanobelt for smart adaptive electronics, Semicond. Sci. Technol. 32 (2017), 104004, https://doi.org/10.1088/1361-6641/aa8605.
[40] S. Bodkhe, P. Ermanni, Challenges in 3D printing of piezoelectric materials, Multifunct. Mater. 2 (2019), 022001, https://doi.org/10.1088/2399-7532/ab0c41.
[41] Y. Wang, R. Wang, S. Wan, Q. Wang, M.J. Kim, D. Ding, W. Wu, Scalable nanomanufacturing and assembly of chiral-chain piezoelectric tellurium nanowires for wearable self-powered cardiovascular monitoring, Nano Futures 3 (2019), 011001, https://doi.org/10.1088/2399-1984/aaf76f.
[42] T.I. Lee, S. Lee, E. Lee, S. Sohn, Y. Lee, S. Lee, G. Moon, D. Kim, Y.S. Kim, J. M. Myoung, Z.L. Wang, High-power density piezoelectric energy harvesting using radially strained ultrathin trigonal tellurium nanowire assembly, Adv. Mater. 25 (2013) 2920–2925, https://doi.org/10.1002/adma.201300657.
[43] K. Wang, Y. Yang, H.-W. Liang, J.-W. Liu, S.-H. Yu, First sub-kilogram-scale synthesis of high quality ultrathin tellurium nanowires, Mater. Horiz. 1 (2014) 338–343, https://doi.org/10.1039/c4mh00004h.
[44] Y. Zhao, X. Wang, S. Yang, E. Kuttner, A.A. Taylor, R. Salemmilani, X. Liu, M. Moskovits, B. Wu, A. Dehestani, J.-F. Li, M.F. Chisholm, Z.-Q. Tian, F.-R. Fan, J. Jiang, G.D. Stucky, Correction to “protecting the nanoscale properties of Ag nanowires with a solution-grown SnO2 monolayer as corrosion inhibitor”, J. Am. Chem. Soc. 141 (2019) 17950, https://doi.org/10.1021/jacs.9b07172.
[45] M. Zeng, D. King, D. Huang, C. Do, L. Wang, M. Chen, S. Lei, P. Lin, Y. Chen, Z. Cheng, Iridescence in nematics: photonic liquid crystals of nanoplates in absence of long-range periodicity, Proc. Natl. Acad. Sci. 116 (2019) 18322–18327, https://doi.org/10.1073/pnas.1906511116.
[46] C. Grigoriadis, H. Duran, M. Steinhart, M. Kappl, H.-J. Butt, G. Floudas, Suppression of phase transitions in a confined rodlike liquid crystal, ACS Nano 5 (2011) 9208–9215, https://doi.org/10.1021/nn203448c.
[47] N. Bridonneau, G. Mattana, V. Noël, S. Zrig, F. Carn, Morphological control of linear particle deposits from the drying of inkjet-printed rivulets, J. Phys. Chem. Lett. 11 (2020) 4559–4563, https://doi.org/10.1021/acs.jpclett.0c01244.
[48] M. Zeng, Y. Zhang, Colloidal nanoparticle inks for printing functional devices: emerging trends and future prospects, J. Mater. Chem. A 7 (2019) 23301–23336, https://doi.org/10.1039/c9ta07552f.
[49] M. Zeng, W. Kuang, I. Khan, D. Huang, Y. Du, M. Saeidi-Javash, L. Zhang, Z. Cheng, A.J. Hoffman, Y. Zhang, Colloidal nanosurfactants for 3D conformal printing of 2D van der Waals materials, Adv. Mater. 32 (2020) 2003081, https://doi.org/10.1002/adma.202003081.
[50] M. Saeidi-Javash, W. Kuang, C. Dun, Y. Zhang, 3D conformal printing and photonic sintering of high-performance flexible thermoelectric films using 2D nanoplates, Adv. Funct. Mater. 29 (2019) 1901930, https://doi.org/10.1002/adfm.201901930.
[51] P. Lee, J. Lee, H. Lee, J. Yeo, S. Hong, K.H. Nam, D. Lee, S.S. Lee, S.H. Ko, Highly stretchable and highly conductive metal electrode by very long metal nanowire percolation network, Adv. Mater. 24 (2012) 3326–3332, https://doi.org/10.1002/adma.201200359.
[52] F. Xu, Y. Zhu, Highly conductive and stretchable silver nanowire conductors, Adv. Mater. 24 (2012) 5117–5122, https://doi.org/10.1002/adma.201201886.
[53] Y. Wang, G. Qiu, R. Wang, S. Huang, Q. Wang, Y. Liu, Y. Du, W.A. Goddard, M. J. Kim, X. Xu, P.D. Ye, W. Wu, Field-effect transistors made from solution-grown two-dimensional tellurene, Nat. Electron 1 (2018) 228–236, https://doi.org/10.1038/s41928-018-0058-4.
[54] J.-H. Lee, K.Y. Lee, B. Kumar, N.T. Tien, N.-E. Lee, S.-W. Kim, Highly sensitive stretchable transparent piezoelectric nanogenerators, Energ. Environ. Sci. 6 (2012) 169–175, https://doi.org/10.1039/c2ee23530g.
[55] Y.S. Jung, H.J. Choi, J.W. Park, Y.S. Cho, Anisotropic in-situ stretching-strain engineering of flexible multilayer thin-film nanogenerators with Cu interlayers, Nano Energy 82 (2021), 105690, https://doi.org/10.1016/j.nanoen.2020.105690.
[56] A. Chortos, Z. Bao, Skin-inspired electronic devices, Mater. Today 17 (2014) 321–331, https://doi.org/10.1016/j.mattod.2014.05.006.
[57] K.C. Pradel, W. Wu, Y. Ding, Z.L. Wang, Solution-derived ZnO homojunction nanowire films on wearable substrates for energy conversion and self-powered gesture recognition, Nano Lett. 14 (2014) 6897–6905, https://doi.org/10.1021/nl5029182.
[58] Z. Liu, S. Zhang, Y.M. Jin, H. Ouyang, Y. Zou, X.X. Wang, L.X. Xie, Z. Li, Flexible piezoelectric nanogenerator in wearable self-powered active sensor for respiration and healthcare monitoring, Semicond. Sci. Technol. 32 (2017), 064004, https://doi.org/10.1088/1361-6641/aa68d1.
[59] Z. Zhou, K. Chen, X. Li, S. Zhang, Y. Wu, Y. Zhou, K. Meng, C. Sun, Q. He, W. Fan, E. Fan, Z. Lin, X. Tan, W. Deng, J. Yang, J. Chen, Sign-to-speech translation using machine-learning-assisted stretchable sensor arrays, Nat. Electron 3 (2020) 571–578, https://doi.org/10.1038/s41928-020-0428-6.
[60] J.R. Sempionatto, M. Lin, L. Yin, E.D. la paz, K. Pei, T. Sonsa-ard, A.N. de, L. Silva, A.A. Khorshed, F. Zhang, N. Tostado, S. Xu, J. Wang, An epidermal patch for the

simultaneous monitoring of haemodynamic and metabolic biomarkers, Nat. Biomed. Eng. (2021) 1–12, https://doi.org/10.1038/s41551-021-00685-1.
[61] C. Dagdeviren, Y. Su, P. Joe, R. Yona, Y. Liu, Y.-S. Kim, Y. Huang, A.R. Damadoran, J. Xia, L.W. Martin, Y. Huang, J.A. Rogers, Conformable amplified lead zirconate titanate sensors with enhanced piezoelectric response for cutaneous pressure monitoring, Nat. Commun. 5 (2014) 4496, https://doi.org/10.1038/ncomms5496.
[62] Z. Liu, Q. Zheng, Y. Shi, L. Xu, Y. Zou, D. Jiang, B. Shi, X. Qu, H. Li, H. Ouyang, R. Liu, Y. Wu, Y. Fan, Z. Li, Flexible and stretchable dual mode nanogenerator for rehabilitation monitoring and information interaction, J. Mater. Chem. B 8 (2020) 3647–3654, https://doi.org/10.1039/c9tb02466b.
[63] M. Zhu, Z. Sun, Z. Zhang, Q. Shi, T. He, H. Liu, T. Chen, C. Lee, Haptic-feedback smart glove as a creative human-machine interface (HMI) for virtual/augmented reality applications, Sci. Adv. 6 (2020) 8693, https://doi.org/10.1126/sciadv.aaz8693.
[64] A.D. Valentine, T.A. Busbee, J.W. Boley, J.R. Raney, A. Chortos, A. Kotikian, J. D. Berrigan, M.F. Durstock, J.A. Lewis, Hybrid 3D printing of soft electronics, Adv. Mater. 29 (2017) 1703817, https://doi.org/10.1002/adma.201703817.
[65] J. Li, Y. Long, F. Yang, H. Wei, Z. Zhang, Y. Wang, J. Wang, C. Li, C. Carlos, Y. Dong, Y. Wu, W. Cai, X. Wang, Multifunctional artificial artery from direct 3D printing with built-in ferroelectricity and tissue-matching modulus for real-time sensing and occlusion monitoring, Adv. Funct. Mater. 30 (2020) 2002868, https://doi.org/10.1002/adfm.202002868.
[66] L. Dong, C. Jin, A.B. Closson, I. Trase, H.R. Richards, Z. Chen, J.X.J. Zhang, Cardiac energy harvesting and sensing based on piezoelectric and triboelectric designs, Nano Energy 76 (2020), 105076, https://doi.org/10.1016/j.nanoen.2020.105076.

Yipu Du is a Ph.D. student in the Department of Aerospace and Mechanical Engineering at the University of Notre Dame. He received his B.S. from Zhejiang University in 2019. His research interests include hybrid additive manufacturing of wearable devices and developing data-driven methods to improve the additive manufacturing capability.

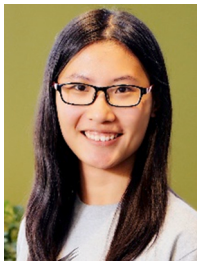

Dr. Ruoxing Wang received her BS degree in Chemistry in 2015 from University of Science and Technology of China (USTC). She received her Ph.D. from School of Industrial Engineering at Purdue University in May 2021, under the supervision of Prof. Wenzhuo Wu. Her research interests mainly focus on nanomanufacturing including the design of functional nanomaterials and fabrication of nanodevices for energy and human-health related applications.

Dr. Minxiang Zeng is a Research Scientist in the Department of Aerospace and Mechanical Engineering at the University of Notre Dame. He received his Ph.D. in Chemical Engineering from Texas A&M University in 2018, and his B.S. from the University of Science and Technology of China in 2014. His research interests include self-assembly of 2D materials, additive manufacturing of functional devices, and development of combinatorial materials.

Shujia Xu received his BS degree in Mechanical Engineering in 2015 form South China University of Technology (SCUT) and his MS degree in Biomedical Engineering in 2018 from Sun Yat-Sen University (SYSU). He is currently a PhD student in Industrial Engineering at Purdue University under the supervision of Prof. Wenzhuo Wu. His research interests mainly focus on ink-based additive manufacturing of flexible electronics for human-integrated applications.

Mortaza Saeidi-Javash is a Ph.D. candidate in the Department of Aerospace and Mechanical Engineering at the University of Notre Dame. He received his M.S. and B.S. degrees in Mechanical Engineering from the University of Oklahoma and University of Tabriz in 2017 and 2012 respectively. His research interests include microscale additive manufacturing of functional devices for energy harvesting and sensing.

Dr. Wenzhuo Wu is the Ravi and Eleanor Talwar Rising Star Associate Professor in the School of Industrial Engineering at Purdue University. He received his B.S. degree in Electrical Engineering from University of Science and Technology of China (USTC) in 2005, and M.S. degree in Electrical Engineering from National University of Singapore (NUS) in 2008. Dr. Wu received his Ph.D. from Georgia Tech in Materials Science and Engineering in 2013. Dr. Wu's research interests include design, manufacturing, and integration of nanomaterials for applications in energy, electronics, quantum technologies, and wearable devices.

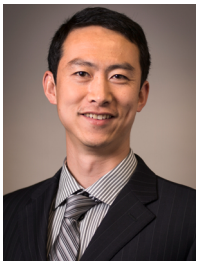

Yanliang Zhang is an Associate Professor in the Department of Aerospace and Mechanical Engineering at University of Notre Dame. He received his Ph.D. in Mechanical Engineering from Rensselaer Polytechnic Institute in 2011, and his M.S. and B.S. from Southeast University in 2008 and 2005. His research focuses on additive manufacturing and scalable nanomanufacturing for sustainable energy and sensor systems, printed electronics, sensors and energy harvesting devices. He has received honors including U.S. National Science Foundation Career Award and Young Investigator Award from International Thermoelectric Society.